Electronic structure of an antiferromagnetic metal: $CaCrO_3$

P. A. Bhobe,[1,2,*] A. Chainani,[2] M. Taguchi,[2] R. Eguchi,[1,2] M. Matsunami,[1,2] T. Ohtsuki,[2] K. Ishizaka,[1] M. Okawa,[1] M. Oura,[2] Y. Senba,[3] H. Ohashi,[3] M. Isobe,[1] Y. Ueda,[1] and S. Shin[1,2]

[1]*Institute for Solid State Physics, The University of Tokyo, Kashiwa, Chiba 277-8581, Japan*

[2]*RIKEN, SPring-8 Centre, Sayo-cho, Sayo-gun, Hyogo 679-5148, Japan*

[3]*JASRI/SPring-8, Sayo-cho, Sayo-gun, Hyogo 679-5198, Japan*

(Received 3 November 2010; revised manuscript received 28 March 2011; published 29 April 2011)

We report on the electronic structure of the perovskite oxide $CaCrO_3$ using valence-band, core-level, and Cr $2p$-$3d$ resonant photoemission spectroscopy (PES). Despite its antiferromagnetic order, a clear Fermi edge characteristic of a metal with dominant Cr $3d$ character is observed in the valence-band spectrum. The Cr $3d$ single-particle density of states are spread over 2 eV, with the photoemission spectral weight distributed in two peaks centered at $\sim$1.2 and 0.2 eV below E_F, suggestive of the coherent and incoherent states resulting from strong electron-electron correlations. Resonant PES across the Cr $2p$-$3d$ threshold identifies a "two-hole" correlation satellite and yields an on-site Coulomb energy $U \sim 4.8$ eV. The metallic DOS at E_F is also reflected through the presence of a well-screened feature at the low binding energy side of the Cr $2p$ core-level spectrum. X-ray-absorption spectroscopy at Cr $L_{3,2}$ and O K edges exhibit small temperature-dependent changes that point toward a small change in Cr-O hybridization. The Cr $2p$ core-level spectrum can be reproduced using cluster model calculations that include a charge transfer from the metallic screening channel at E_F. The overall results indicate that $CaCrO_3$ is a strongly hybridized antiferromagnetic metal, lying in the regime intermediate to Mott-Hubbard and charge-transfer systems.

DOI: 10.1103/PhysRevB.83.165132 PACS number(s): 79.60.−i, 71.27.+a, 71.30.+h

I. INTRODUCTION

The origin of band gaps and character of the valence electrons in $3d$ transition-metal compounds have been central to the description of correlated electron systems. Transition metal oxides, in particular, continue to play a fascinating role in the field of condensed matter physics, based on their exotic physical properties, such as high-Tc superconductivity in cuprates,[1] one-dimensional charge and spin self-organization in nickelates,[2] and charge and orbital ordering in manganites.[3] Numerous efforts to elucidate the underlying physics led to a broad classification scheme of such materials into two categories, viz. the Mott-Hubbard type and the charge-transfer type.[4] The compounds of early transition metals such as Ti and V are thought to be Mott-Hubbard type, while the compounds of late transition metals like Ni and Cu form the charge-transfer type. The basis for such a classification stands on the relative value of the Coulomb interaction energy U between the d electrons and the one-electron bandwidth W. In the limit of large U, this system of singly occupied sites can be described by the antiferromagnetic (AF) Heisenberg spin Hamiltonian. The opposite limit of large W, on the other hand, gives an uncorrelated half filled metallic band. In other words, a system becomes metallic when $U/W \ll 1$ and insulating when $U/W \gg 1$. A transition from nonmagnetic metal to an AF insulator is thus expected to occur as U/W is varied within this picture. V_2O_3 is the most widely studied example with a low-temperature AF insulating phase, which transforms into a high-temperature paramagnetic metal.[5] However, studies over the last decade have identified several strongly correlated systems that exhibit an AF metal ground state. These systems seem to be characterized by strong hybridization of the metal $3d$ and ligand $2p$ states, leading to an intermediate U/W. Examples include $(La_{1-z}Nd_z)_{1-x}Sr_xMnO_3$,[6] $Pr_{0.5}Sr_{0.5}MnO_3$,[7] CrN,[8] CrB_2,[9] $CaFe_2As_2$,[10] $BaFe_2As_2$,[11] etc. These experimental results were preceded by the theoretical studies on the Hubbard model in the dynamic mean-field approximation.[5] In particular, the work of Rozenberg *et al.*[5] identified an AF metal phase between the paramagnetic metal phase and the AF insulating phase, in the T/W versus U/W phase diagram (where T is the temperature, W is the effective bandwidth, U is the on-site Coulomb energy). The phase diagram was obtained as a solution to the Hubbard model based on dynamic mean-field theory (DMFT) and showed that at low T, the Mott-Hubbard metal-insulator transition occurs at an intermediate $U_c \sim 3W$. It was also shown that the same theory accounted very nicely for the optical conductivity spectra of the paramagnetic metal and AF insulator phases of V_2O_3.

Yet another exciting compound possibly belonging to this family is the Cr^{4+} based perovskite: $CaCrO_3$. This $GdFeO_3$-type distorted perovskite has an orthorhombic structure with *Pbnm* space group, and orders antiferromagnetically at $T_N \sim 90$ K.[12] The magnetic structure is C type, i.e., ferromagnetic chains along the c direction stacked antiferromagnetically, with a magnetic moment of $1.2\mu_B$, as determined from neutron diffraction.[12] Moreover, neutron-diffraction study also revealed the pronounced structural distortion taking place at T_N with contraction along the c axis and expansion along the a and b axes. The electronic nature of this material is quite ambiguous, as reflected by its electrical transport studies. Based on the observation of a rise in electrical resistivity with a fall in temperature, polycrystalline $CaCrO_3$ was first proposed to be a semiconductor.[13] Subsequent report on single crystals showed a decrease in resistivity with the fall in temperature stating it to be a metal.[14] Recently, a pressure-dependent electrical resistivity study of $CaCrO_3$ and $SrCrO_3$ proposed that these compounds are semiconductors at ambient pressure, which undergo a transition to a metal with increase in pressure.[15] On

the other hand, a subsequent study using infrared reflectivity measurements point to a three-dimensional metallic nature and highlights the importance of correlation effects, stating $CaCrO_3$ to be itinerant but close to being localized.[12] Efforts to calculate the electronic density of states (DOS) of $CaCrO_3$ have been made using the local spin-density approximation (LSDA) and LSDA+U (U: on-site Coulomb correlations).[16] A metallic behavior with Stoner-like band magnetism is found using the LSDA approach, whereas LSDA+U results show an insulating ground state with (i) a small gap of 0.05 eV for calculations that adhere to the actual crystal symmetry and (ii) a robust gap of 0.5 eV for a symmetry unrestricted approach, indicating that the calculated DOS for $CaCrO_3$ is quite sensitive to its crystal symmetry.[16] The magnetic order in this case results from a superexchange interaction of localized electrons. It is evident that the key to resolve the ambiguity raised over the electronic ground state of $CaCrO_3$ lies in understanding the character of d electrons and the possible role of Coulomb correlations. Therefore a knowledge of the electronic structure of $CaCrO_3$ using spectroscopic experiments that reflect the Cr 3d states is essential.

The present study thus aims to address the nature of the electronic structure and identify the role of correlations in $CaCrO_3$ using soft x rays and laser photoemission spectroscopy (PES). We establish that $CaCrO_3$ is an antiferromagnetic metal with large on-site electron correlation energy U. We also show that it is the sizable hybridization between Cr 3d and O 2p that prevents $CaCrO_3$ from being an insulator in spite of the strong correlations. In particular, we have carried out resonant PES with excitation energy tuned across the Cr 2$p \rightarrow$ 3d threshold, the valence band (VB), Cr 2p, Ca 2p, and O 1s core-level spectra at 25 K, i.e., in the antiferromagnetically ordered state, using synchrotron radiation. Resonant PES is a useful technique to reveal the transition-metal 3d electron character in the total VB, as it provides site-projected and orbital-selective 3d partial DOS.[17] Further, while the metallicity in $CaCrO_3$ is confirmed by its valence-band and core-level spectra, resonant PES shows the presence of strong Coulomb correlations in $CaCrO_3$. In addition, x-ray-absorption spectroscopy (XAS) has been carried out in the high-temperature paramagnetic phase at 120 K and the low-temperature antiferromagnetically ordered phase at 25 K, across the Cr $L_{3,2}$ edge and O K edge. XAS shows small temperature-dependent changes across T_N thus revealing the effect of structural distortion in the form of small changes in the Cr 3d–O 2p hybridization.

II. EXPERIMENTAL DETAILS

Polycrystalline $CaCrO_3$ used in the present study was prepared by high-pressure synthesis as described in Ref. 12. The XRD pattern of the sample agreed with previously published data[12] thus confirming its crystalline phase purity. The AF transition was confirmed to be at $T_N = 90$ K by the magnetic susceptibility measurements.[12] Soft x-ray photoemission and XAS experiments were performed on $CaCrO_3$ at BL17SU SPring-8. The data were obtained using Gammadata-Scienta SES2002 electron analyzer. The total-energy resolution for PES was ~200 meV and the data were collected in the angle-integrated mode. Resonant PES spectra were normalized to scan time and incident photon flux. XAS was recorded in the total electron yield mode. Laser PES was performed using a Scienta R4000WAL electron analyzer and a vacuum-ultraviolet laser ($h\nu = 6.994$ eV),[18] and the total energy resolution was set to 5 meV at 10 K. All the measurements were carried out on a clean sample surface obtained by fracturing the sample *in situ* at the lowest temperature of measurement. A vacuum below 4×10^{-8} Pa was maintained throughout the measurements. All the spectra were calibrated using the Fermi level obtained for a gold film evaporated onto the sample holder. We have estimated the stoichiometry of our sample from the Ca 2p, Cr 2p, and O 1s core-level spectra reported in this study. From the relative intensity divided by the atomic sensitivity factors, we estimate the ratios of $1(\pm 0.01) : 1.01(\pm 0.02) : 3(\pm 0.02)$, for Ca, Cr, and O respectively. The terms in the bracket indicate the experimental error. The results indicate that our samples are consistent with the nominal composition.

III. RESULTS AND DISCUSSION

Figures 1(a) and 1(b) presents the Ca 2p and O 1s core-level spectra obtained using 1200 eV incident photon energy. Sharp and clean spectra with no spurious features at the higher binding energy (BE) side of the main peak confirm the high quality of the sample surface. The Ca 2p spectrum exhibits a BE typical of Ca^{2+} ($\equiv$ 345 eV), but with an overall asymmetric (Doniach- Šunjić) line shape, as is evident from the fit in Fig. 1(a). Such asymmetric line shape is an outcome of the electron-hole pair shake-up process that is characteristic of a metal.[19] The O 1s has a BE of 528.5 ± 0.2 eV that matches with the value of 529.3 eV reported for another Cr^{4+} compound, CrO_2.[20] Similar to Ca 2p, a single asymmetric peak provides a good fit to the O 1s peak. The fairly broad spectrum, however, hints toward more than one component contributing toward the total intensity of the O 1s signal. It is well established from the neutron and x-ray

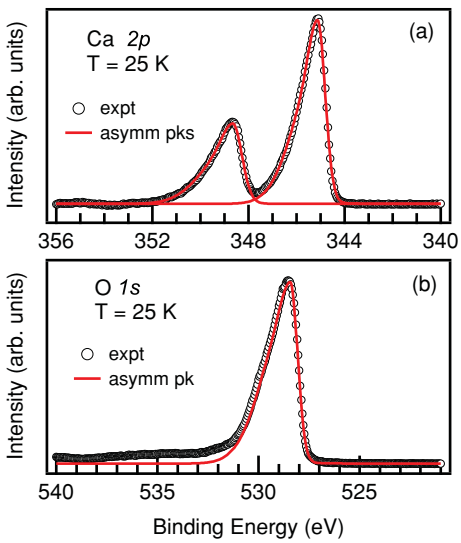

FIG. 1. (Color online) (a) Ca 2p and (b) O 1s core-level spectra obtained using 1200-eV excitation energy. The spectra can be fitted with asymmetric (Doniach- Šunjić) line-shape peaks.

powder-diffraction studies of $CaCrO_3$ (Refs. 12 and 15) that the room-temperature *Pbnm* structure undergoes distortion simultaneous to the magnetic ordering at $T_N \sim 90$ K. As a result, the lattice parameter along the *c* axis shrinks, while that along *a* and *b* elongate, yielding three different Cr-O bond distances; with the apical bond Cr-O1 = 1.8954(5)Å, and the in-plane bonds Cr-O2 = 1.901(6)Å and 1.919(5)Å (as stated in Ref. 15). We thus have three different types of oxygen ions contributing toward the total O 1*s* spectrum that can result in one broad signal. We confirm the metallic behavior from the VB measurements in the following.

The VB spectrum of $CaCrO_3$ in the antiferromagnetically ordered phase is presented in Fig. 2(a). A clear signature of metallicity is observed as the spectral intensity crosses the Fermi edge (E_F) indicating the presence of finite density of states (DOS) at E_F. This is an interesting result as the commonly known metallic oxides are either correlated paramagnets [for example, $LaNiO_3$ (Ref. 21)] or ferromagnets [for example, CrO_2,[22] $SrRuO_3$ (Ref. 23)]. Besides, though a rise in electrical resistivity was observed with the lowering of temperature in polycrystalline $CaCrO_3$, an activation energy could not be extracted.[12,13,15] In fact, the metallic nature of the antiferromagnetic phase of $CaCrO_3$ was also deduced from its infrared reflectivity and optical conductivity measurements.[12] Comparing the experimental VB with the reported band-structure calculations (LSDA+U approach),[12,16] the peak centered at ~1.2 eV below E_F can be attributed to the Cr 3*d* states. While the broad band centered at ~6 eV below E_F comprises dominantly of the O 2*p* states.

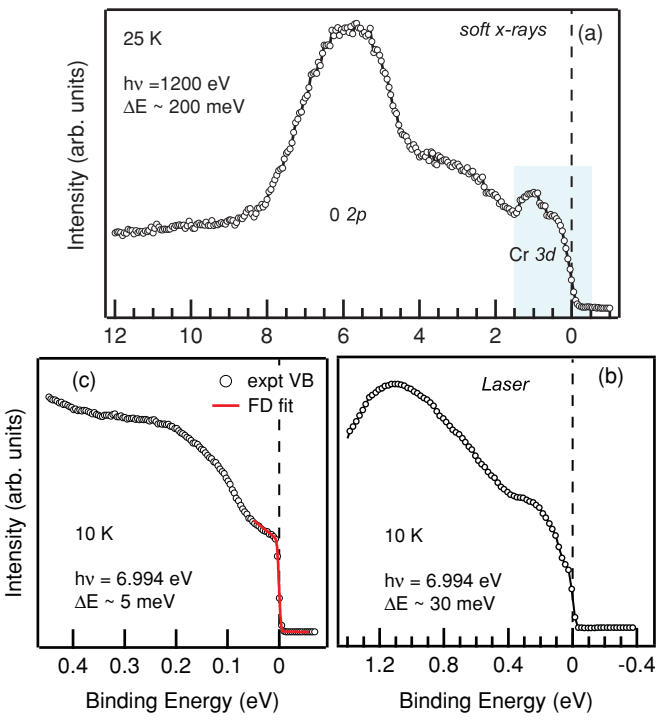

FIG. 2. (Color online) (a) Soft x-ray VB spectrum of $CaCrO_3$ obtained at 25 K. A clear metallic Fermi edge can be seen. The shaded portion was scanned using laser source and the corresponding VB spectrum is shown in (b). The feature at 0.2 eV is clearly seen. (c) Resolution-convoluted Fermi-Dirac function (solid line) fit to the experimental VB.

In order to ascertain the low-energy scale electronic structure of $CaCrO_3$ in the vicinity of E_F, we measured bulk sensitive laser PES at 10 K using an excitation energy of $h\nu = 6.994$ eV and 5 meV resolution [see Figs. 2(b) and 2(c)]. Apart from the sharp Fermi edge, which reiterates the metallic nature of $CaCrO_3$, laser VB depicts a clear hump around 0.2 eV below E_F. Thus it appears that the spectral weight of the Cr 3*d* band dominant at E_F is distributed in peaks centered at ~1.2 and ~0.2 eV BE. Similar features have been reported in the VB of early transition-metal oxides such as $Ca_{1-x}Sr_xVO_3$, $Y_{1-x}Ca_xTiO_3$, leading to their classification as Mott-Hubbard correlated metals.[24–26] In these materials the feature very near to E_F has been attributed to the itinerant *d*-band states or coherent part of the spectral function, while that present at higher BE has been assigned to the incoherent part or the lower Hubbard band and corresponds to electronic states localized due to electron-electron correlations. Additionally, LSDA calculations[12,16] predict the Cr 3*d* states to occur at <1 eV BE, while it is evident from Fig. 2 that the bandwidth of Cr 3*d* is spread over 2 eV. Hence the experimental VB spectrum obtained here suggests a picture that goes beyond the LSDA calculations.

In light of such reasoning, inclusion of electron-electron correlation effect in band-structure calculations seems imperative for the description of electronic structure of $CaCrO_3$. In this regard, the LSDA+U calculations reported so far[16] show that the calculated DOS for $CaCrO_3$ is quite sensitive to its crystal structure. In their report, Streltsov *et al.*[16] state that the total DOS obtained with the full set of the *Pbnm* crystal symmetry operations results in a small gap of 0.05 eV and slight changes in the basis set or calculation parameters like U result in the closing of the gap. On the other hand, an insulating ground state with a gap of 0.5 eV and orbital ordering is observed for a symmetry unrestricted calculation. This band gap is very robust and persists even if U is decreased down to 1.8 eV. Irrespective of the choice of solution based on crystal symmetry, it is found that the introduction of on-site Coulomb correlations leads to a strong mixing of occupied Cr 3*d* and O 2*p* states. The same study also noted that the magnetic interactions are governed by sizable *pd* hybridization. Having observed a clear metallic Fermi edge, the experimental data suggests that the LSDA+U results obtained using full crystal symmetry provides a better description of the experimental VB spectrum. However, it becomes important to obtain an estimate of U from the experimental data. Accordingly, resonant VB spectra were obtained by tuning the excitation energy across the Cr 2*p*-3*d* absorption, which significantly increases the relative photoemission cross section of Cr 3*d* states over O 2*p* states. In order to obtain the resonant PES, we first measured the XAS across the Cr $L_{3,2}$ edge. We have also carried out measurements at the O *K* edge above and below T_N.

Figure 3(a) presents the O *K*-edge XAS that originates from transition to unoccupied O 2*p* states hybridized with the metal states and hence reflects features of metal 3*d* character.[27] Given that Cr^{4+} in $CaCrO_3$ has a d^2 configuration, the first peak around 528 eV can be assigned to the relatively empty t_{2g} band. Above the t_{2g}, one can see an empty e_g band centered at ~530 eV. An energy separation of ~2.1 eV between these two peaks is an estimate of the crystal-field parameter, $10Dq$. Figure 3(a) also shows the temperature

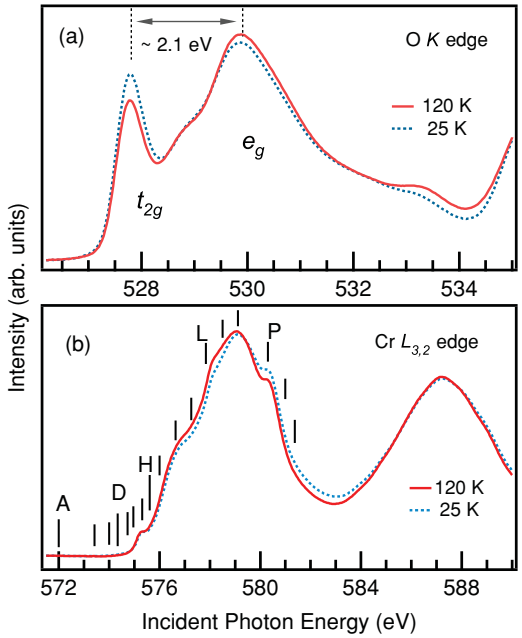

FIG. 3. (Color online) XAS measured as a function of temperature above and below antiferromagnetic ordering temperature T_N = 90 K. (a) O K edge and (b) Cr $L_{3,2}$ edge. Temperature-dependent changes are seen in both the spectra.

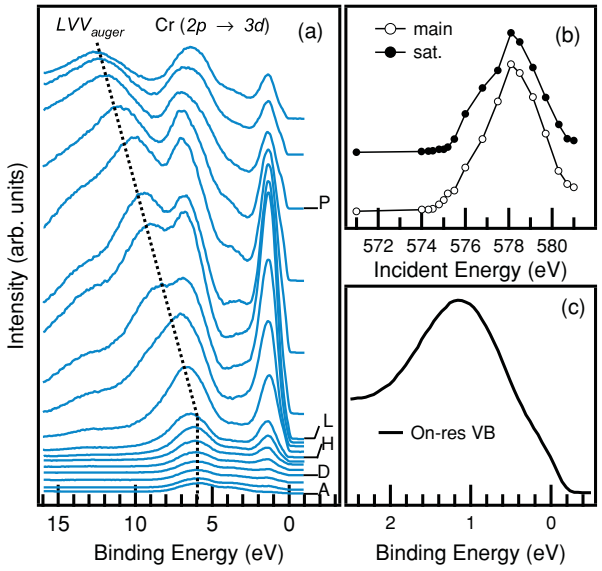

FIG. 4. (Color online) (a) The resonant PES VB spectra recorded using excitation photon energy across Cr $2p$-$3d$ transition. Dotted line shows the evolution of the satellite feature into the Auger feature. (b) CIS for the main Cr $3d$ peak at 1.2 eV and the satellite feature at 5.9 eV, normalized to the intensity obtained for $h\nu = 571$ eV spectrum and have arbitrary offset. (c) On-resonance VB reiterates the two-peak structure of Cr dominated states at E_F with features at 1.2 and 0.2 eV.

dependence of O K edge where an increase in the relative intensity of the first peak is seen at low temperature. Such an increase in the first peak intensity hints toward a small increase of O $2p$–Cr $3d$ hybridization in the low-temperature phase. A small but definite temperature-dependent change is simultaneously observed in the Cr $L_{3,2}$-edge XAS, as seen in Fig. 3(b). While the spectrum for the Cr $L_{3,2}$ edge consists of many multiplets, certain features (especially those indicated with "L" and "P") display a clear change in spectral weight on decreasing temperature. The difference in the apical and in-plane Cr-O bond distances known from low-temperature crystal structure studies[12,15] are considered responsible for such a spectral weight transfer.

Next, we consider the presence of electron-electron correlations in $CaCrO_3$. The resonant VB spectra shown in Fig. 4(a) were recorded with excitation energy ranging from 571 to 581 eV. The actual incident photon energies are indicated by tick marks on the Cr L_3 XAS curve presented in Fig. 3(b). The relative photoionization cross section of Cr $3d$ to O $2p$ being significantly increased, the 1.2-eV peak is enhanced with the increasing photon energy. Further, an Auger signal (LVV_{auger}) with an apparent binding energy of about 11.7 eV for the maximum incident photon energy spectrum (topmost curve) can be easily identified by its dependence on the excitation energy. The Auger feature converges toward the satellite peak at ~5.9 eV for the lower incident photon energy (the dotted line shows the convergence of the Auger peak). Constant-initial-state (CIS) spectra of the main peak (1.2 eV) and the Auger peak are presented in Fig. 4(b). These spectra follow the same photon energy dependence as Cr L_3 XAS curve, thus indicating that the Cr $3d$ weight is indeed spread over a wide energy range. It also serves to confirm the Cr $3d$ character of the so-called two-hole correlation satellite.[28] These observations indicate the presence of strong on-site Coulomb interaction energy (U) in $CaCrO_3$, as has been demonstrated for Cr metal,[28] Cr silicide,[29] and Cr nitride.[8] Besides, the VB spectrum obtained with excitation energy equal to the maximum of Cr L_3 XAS, i.e., the *on-res* VB spectrum, shown in Fig. 4(c) emulates the laser VB spectrum with a two-peak structure of Cr $3d$ states with a main peak at 1.2 eV and a weak shoulder at ~0.2 eV. By employing an analysis similar to that of CrN,[8] we obtain an estimate of electron-electron correlation energy in $CaCrO_3$. The expression to obtain U can be stated as

$$U = E_{2p} - (h\nu - BE_{\text{auger}}) - 2\epsilon_{3d}$$

where E_{2p} is the binding energy of Cr $2p$, $h\nu$ is the incident photon energy, and BE_{auger} gives the BE of the corresponding Auger peak. $2\epsilon_{3d}$ is the average energy of two uncorrelated holes, obtained from the self-convolution of the one-electron removal Cr $3d$ peak occurring at 1.2 eV. On substituting the experimental values of $E_{2p} = 576.5$ eV, obtained as the BE of main peak in the Cr $2p$ spectrum [Fig. 5(b)], $(h\nu - \text{BE}_{\text{auger}}) =$ 569.33 eV and $2\epsilon_{3d} \sim 2.4$ eV, we obtain an estimate of $U \sim 4.8$ eV for $CaCrO_3$. Thus summing up the experimental results presented so far, we establish that $CaCrO_3$ is an antiferromagnetic metal with large on-site electron correlation energy, U.

Finally, the Cr $3s$ and $2p$ core-level spectra of $CaCrO_3$ at $T = 25$ K is presented in Figs. 5(a) and 5(b), respectively. As is clear from the fitting, the $3s$ spectrum exhibits a doublet with energy separation of about 3.35 eV. Such multiplet splitting of $3s$ core-level in transition-metal compounds primarily originates from the exchange coupling between the s core hole spin and the $3d$ spin. It is expressed as $\Delta E = (2S + 1)J_{sd}$ where S is the magnitude of total spin

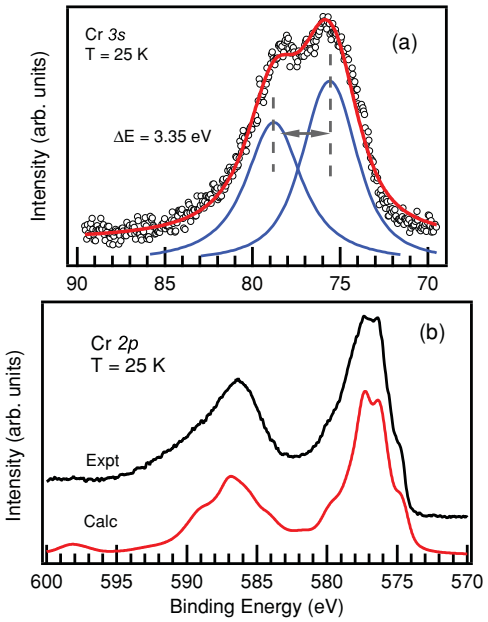

FIG. 5. (Color online) Core-level spectra of (a) Cr 3s showing the doublet feature separated by 3.35 eV and (b) Cr 2p showing multiplet features. The calculated spectrum for Cr 2p is obtained using cluster model calculations including metallic screening channel at E_F. The charge-transfer energy Δ is set to 3 eV and the energy of metallic screening channel Δ^* is set to zero. (See text for more details.)

of the 3d electrons and J_{sd} denotes the effective exchange integral between the 3s core hole and the 3d electron. The splitting of 3s spectrum hence reflects a well-defined local magnetic moment of the corresponding transition metal ion, as is known for many transition metal compounds.[30–35] Such a splitting is observed in insulating Cr_2O_3 (= 3.8 eV) as well as in metallic CrO_2 (= 3.5 eV), both of which possess a local moment, whereas it is absent in diamagnetic $K_2Cr_2O_7$.[20]

The Cr 2p spectrum presented in Fig. 5(b) also shows multiplet features besides the $2p_{3/2}$,$2p_{1/2}$ spin-orbit splitting. The BE of the features in $2p_{3/2}$ main peak are ~577.3 and 576.5 eV. The multiplet splitting of Cr $2p_{3/2}$ due to exchange coupling has also been reported for insulating compounds like Cr based sulphides and selenides, where a moment of 2.9–3.0μ_B results in a splitting of 0.95–1.0 eV.[36] In addition, a feature is observed at 575 eV, on the low BE side of the main peak in the 2p core-level spectrum. The occurrence of such a low BE feature in transition-metal compounds has been attributed to final-state screening effects that come to fore when electronic states are present at E_F, indicative of the metallic nature of the compound.[37–40] In very simple terms, a well-screened feature develops due to the core-hole potential in the photoemission final state being screened by the charge transfer from the conduction-band states at E_F.

With the aim of accounting for the origin of features present in the core-level spectrum of $CaCrO_3$, we have carried out cluster model calculations following the procedure originally described in Ref. 38. In addition to the usual calculations based on a CrO_6 cluster, we introduced a charge transfer from a coherent band C at E_F.[39,40] Such a charge transfer from the coherent states can be directly related to the metallic screening in the core-level PES. Analogous to the parameters associated with Cr 3d and O 2p ligand states viz. charge-transfer energy Δ and hybridization V, the additional parameters were Δ^*, the charge-transfer energy between Cr 3d and C, and V^*, the hybridization between Cr 3d and C. The other parameters involved in the calculations were the on-site Coulomb interaction energy U(≡ 4.5 eV, obtained from the resonant PES above), the crystal-field splitting $10Dq$ (≡ 2.1 eV, obtained from O K-edge XAS), Coulomb interaction between Cr 3d and Cr 2p core-hole states U_{dc} (typically set to 1.2–1.4U). Under these constraints we varied V, V^*, Δ, and Δ^*, and found satisfactory results for $V = 2.9$ eV, $V^* = 0.87$ eV with $\Delta = 3$ eV, and $\Delta^* = 0$, i.e., $\Delta - \Delta^* = 3$ eV. We were able to nicely reproduce the well-screened peak and all the higher BE multiplet features in the calculated spectrum of Cr 2p core level, as seen in Fig. 5(b).

Further, using the same set of parameters, we calculated the Cr $L_{3,2}$-edge XAS spectrum, as presented in Fig. 6. Though the main peaks show resemblance with the experimental data, not all shoulder features are well reproduced. One possible reason for this discrepancy could be the essential difference involved in the process of photoemission and the x-ray absorption. While PES of Cr 2p core-level is strongly dependent on final states derived from ligand screening and metallic screening, the Cr 2p-3d absorption process is essentially an on-site excitation. In fact, the recent LSDA+U study[12,16] proposes a negative Δ as the possible ground state for $CaCrO_3$. Such a proposition is particularly true in the presence of strong hybridization as is also known for other systems like $NaCuO_2$,[41] CrO_2,[42] $CuFeS_2$,[43] While further studies taking into account all these aspects could provide a more definitive picture, it is beyond the scope of the present cluster calculations.

In terms of the overall electronic structure, it is noted that the optical conductivity spectrum of $CaCrO_3$ (Ref. 12) is very similar to that of V_2O_3 (Ref. 5) in the metal phase. Both materials show a Drude-type feature at low energy (< 200 meV) due to excitations of the coherent states, an intermediate or mid-infrared (IR) feature at 0.2–0.7 eV, and the high-energy states (>0.7 eV) arising from excitations

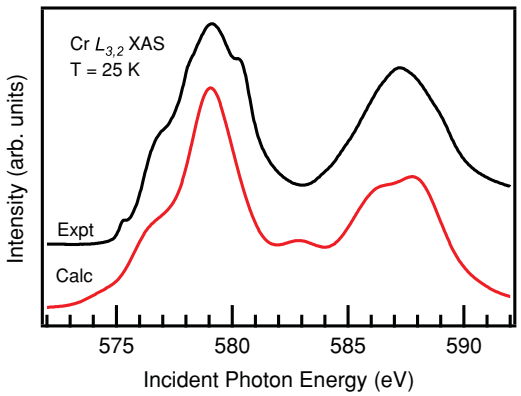

FIG. 6. (Color online) Cr $L_{3,2}$-edge XAS spectrum compared with the calculated spectra obtained using cluster model calculations with inclusion of metallic screening channel at E_F.

between the lower and upper Hubbard bands. As discussed in the introduction, DMFT results showed a quantitative match with the experiments, thus establishing the role of strong correlations in the metallic phase of V_2O_3. Given the similarity of spectral features of $CaCrO_3$, by analogy a similar picture holds for $CaCrO_3$ but for a lower effective U/W corresponding to the AF metal phase in the phase diagram of Ref. 5. Further, the electronic structure calculations by Streltsov *et al.*[16] indicated the importance of $CaCrO_3$ being at a crossover from localized to itinerant behavior. Streltsov *et al.* also discussed the importance of next-nearest-neighbor exchange (in LSDA) or superexchange interaction (in LSDA+U), as responsible for stabilizing the AF metal phase with an intermediate U. The reduced U value was attributed to the large Hund's coupling and the three dimensionality of $CaCrO_3$. We also note that while $V_{2-y}O_3$ also shows an AF metal phase but for which the T_N changes with stoichiometry,[44] the fact that a constant value of T_N (= 90 K) for $CaCrO_3$ samples synthesized and measured by four different groups[12–15] indicates the intrinsic antiferromagnetism in $CaCrO_3$, which is linked to its metallic character. Hence it bears direct relation with the AF metal phase originally identified by Rozenberg *et al.*[5] in the phase diagram of the Hubbard model solved using dynamical mean-field theory. Thus although the dc electrical resistivity of $CaCrO_3$ showed a negative temperature coefficient,[12,13] the resistivity at low temperature extrapolates to a finite value, suggesting a bad metal behavior in the presence of comparable values of bandwidth and on-site Coulomb correlations. Finally, the optical reflectivity[12] approaches unity at $\omega \rightarrow 0$, typical of a three-dimensional metallic behavior.

IV. CONCLUSION

To summarize, our photoemission spectroscopy measurements on $CaCrO_3$ clear the ambiguity cast over its electronic structure from electrical transport measurements. The valence-band spectrum shows a clear Fermi edge, confirming the metallic nature of $CaCrO_3$ in the low-temperature phase. In the vicinity of E_F, the Cr 3d dominated band exhibits a two-peak feature attributable to the localized and itinerant d-band states, quite like the Mott-Hubbard-type systems. Analysis of resonant PES across the Cr $2p \rightarrow 3d$ threshold yields an on-site Coulomb energy $U \sim 4.8$ eV, indicating the presence of strong electron-electron correlations. In spite of the large U, the system is metallic in the antiferromagnetically ordered low-temperature phase. The small temperature-dependent changes observed in Cr $L_{3,2}$ and O K-edge XAS are consistent with a small change in the Cr 3d–O 2p hybridization. The Cr 2p core-level spectrum can be reproduced using cluster model calculations that include a charge transfer from metallic screening channel at E_F. The results indicate that $CaCrO_3$ can be best described as a strongly hybridized antiferromagnetic metal exhibiting a mixed Mott-Hubbard and charge-transfer character.

ACKNOWLEDGMENTS

P. A. Bhobe acknowledges support from Japan Society for Promotion of Science (JSPS). The synchrotron radiation experiments were performed at BL17SU, SPring-8 with the approval of RIKEN (Proposal No. 20091140). Y.U. thanks the JSPS for the Grant-in-Aid for Scientific Research (Grant No. 22244041).

*preeti@spring8.or.jp; pbhobe@gmail.com

[1] J. G. Bednorz and K. A. Muller, Z. Phys. B **64**, 189 (1986).
[2] J. M. Tranquada, B. J. Sternlieb, J. D. Axe, Y. Nakamura, and S. Uchida, Nature (London) **375**, 561 (1995).
[3] Y. Tokura and N. Nagaosa, Science **288**, 462 (2000).
[4] J. Zaanen, G. A. Sawatzky, and J. W. Allen, Phys. Rev. Lett. **55**, 418 (1985).
[5] M. J. Rozenberg, G. Kotliar, H. Kajueter, G. A. Thomas, D. H. Rapkine, J. M. Honig, and P. Metcalf, Phys. Rev. Lett. **75**, 105 (1995).
[6] T. Akimoto, Y. Maruyama, Y. Moritomo, A. Nakamura, K. Hirota, K. Ohoyama, and M. Ohashi, Phys. Rev. B **57**, R5594 (1998).
[7] R. Kajimoto, H. Yoshizawa, Y. Tomioka, and Y. Tokura, Phys. Rev. B **66**, 180402(R) (2002).
[8] P. A. Bhobe, A. Chainani, M. Taguchi, T. Takeuchi, R. Eguchi, M. Matsunami, K. Ishizaka, Y. Takata, M. Oura, Y. Senba, H. Ohashi, Y. Nishino, M. Yabashi, K. Tamasaku, T. Ishikawa, K. Takenaka, H. Takagi, and S. Shin, Phys. Rev. Lett. **104**, 236404 (2010).
[9] G. E. Grechnev, A. S. Panfilov, A. V. Fedorchenko, V. B. Filippov, A. B. Lyashchenko, and A. N. Vasiliev, Low Temp. Phys. **35**, 531 (2009).
[10] S. O. Diallo, V. P. Antropov, T. G. Perring, C. Broholm, J. J. Pulikkotil, N. Ni, S. L. Budko, P. C. Canfield, A. Kreyssig, A. I. Goldman, and R. J. McQueeney, Phys. Rev. Lett. **102**, 187206 (2009).
[11] James G. Analytis, Ross D. McDonald, Jiun-Haw Chu, Scott C. Riggs, Alimamy F. Bangura, Chris Kucharczyk, Michelle Johannes, and I. R. Fisher, Phys. Rev. B **80**, 064507 (2009).
[12] A. C. Komarek, S. V. Streltsov, M. Isobe, T. Möller, M. Hoelzel, A. Senyshyn, D. Trots, M. T. Fernández-Díaz, T. Hansen, H. Gotou, T. Yagi, Y. Ueda, V. I. Anisimov, M. Grüninger, D. I. Khomskii, and M. Braden, Phys. Rev. Lett. **101**, 167204 (2008).
[13] J. B. Goodenough, J. M. Longo, and J. A. Kafalas, Mater. Res. Bull. **3**, 471 (1968).
[14] J. F. Weiher, B. L. Chamberland, and J. L. Gillson, J. Solid State Chem. **3**, 529 (1971).
[15] J.-S. Zhou, C.-Q. Jin, Y.-W. Long, L.-X. Yang, and J. B. Goodenough, Phys. Rev. Lett. **96**, 046408 (2006).
[16] S. V. Streltsov, M. A. Korotin, V. I. Anisimov, and D. I. Khomskii, Phys. Rev. B **78**, 054425 (2008).
[17] S. J. Oh, J. W. Allen, I. Lindau, and J. C. Mikkelsen Jr., Phys. Rev. B **26**, 4845 (1982); L. H. Tjeng, C. T. Chen, J. Ghijsen, P. Rudolf, and F. Sette, Phys. Rev. Lett. **67**, 501 (1991).

[18]T. Kiss, F. Kanetaka, T. Yokoya, T. Shimojima, K. Kanai, S. Shin, Y. Onuki, T. Togashi, C. Zhang, C. T. Chen, and S. Watanabe, Phys. Rev. Lett. **94**, 057001 (2005).
[19]S. Doniach and M. Šunjić, J. Phys. C **3**, 285 (1970); P. S. Cornaglia and A. Georges, Phys. Rev. B **75**, 115112 (2007).
[20]I. Ikemoto, K. Ishii, S. Kinoshita, H. Kuroda, M. A. Alario Franco, and J. M. Thomas, J. Solid State Chem. **17**, 425 (1976).
[21]K. Sreedhar, J. M. Honig, M. Darwin, M. McElfresh, P. M. Shand, J. Xu, B. C. Crooker, and J. Spalek, Phys. Rev. B **46**, 6382 (1992).
[22]R. A. deGroot, F. M. Mueller, P. G. van Engen, and K. H. J. Buschow, Phys. Rev. Lett. **50**, 2024 (1983).
[23]L. Klein, J. S. Dodge, C. H. Ahn, J. W. Reiner, L. Mieville, T. H. Geballe, M. R. Beasley, and A. Kapitulnik, J. Phys.: Condens. Matter **8**, 10111 (1996).
[24]K. Morikawa, T. Mizokawa, K. Kobayashi, A. Fujimori, H. Eisaki, S. Uchida, F. Iga, and Y. Nishihara, Phys. Rev. B **52**, 13711 (1995).
[25]I. H. Inoue, I. Hase, Y. Aiura, A. Fujimori, Y. Haruyama, T. Maruyama, and Y. Nishihara, Phys. Rev. Lett. **74**, 2539 (1995).
[26]K. Morikawa, T. Mizokawa, A. Fujimori, Y. Taguchi, and Y. Tokura, Phys. Rev. B **54**, 8446 (1996).
[27]J. van Elp and A. Tanaka, Phys. Rev. B **60**, 5331 (1999).
[28]S. Hüfner, S.-H. Yang, B. S. Mun, C. S. Fadley, J. Schäfer, E. Rotenberg, and S. D. Kevan, Phys. Rev. B **61**, 12582 (2000).
[29]L. Galán, M. García, J. M. Ripalda, I. Montero, E. Román, D. R. Batchelor, and P. R. Bressler, Appl. Phys. Lett. **84**, 4433 (2004).
[30]C. S. Fadley, D. A. Shirley, A. J. Freeman, P. S. Bagus, and J. V. Mallow, Phys. Rev. Lett. **23**, 1397 (1969); C. S. Fadley and D. A. Shirley, Phys. Rev. A **2**, 1109 (1970).
[31]G. H. Gweon, J. G. Park, and S. J. Oh, Phys. Rev. B **48**, 7825 (1993).
[32]L. Sangaletti, L. E. Depero, P. S. Bagus, and F. Parmigiani, Chem. Phys. Lett. **245**, 463 (1995).
[33]T. Saitoh, A. E. Bocquet, T. Mizokawa, H. Namatame, A. Fujimori, M. Abbate, Y. Takeda, and M. Takano, Phys. Rev. B **51**, 13942 (1995).
[34]V. R. Galakhov, M. Demeter, S. Bartkowski, M. Neumann, N. A. Ovechkina, E. Z. Kurmaev, N. I. Lobachevskaya, Y. M. Mukowskii, J. Mitchell, and D. L. Ederer, Phys. Rev. B **65**, 113102 (2002).
[35]N. Mannella, C. H. Booth, A. Rosenhahn, B. C. Sell, A. Nambu, S. Marchesini, B. S. Mun, S.-H. Yang, M. Watanabe, K. Ibrahim, E. Arenholz, A. Young, J. Guo, Y. Tomioka, and C. S. Fadley, Phys. Rev. B **77**, 125134 (2008).
[36]V. Tsurkan, St. Plogmann, M. Demeter, D. Hartmann, and M. Neumann, Eur. Phys. J. B **15**, 401 (2000).
[37]A. Kotani and Y. Toyozawa, J. Phys. Soc. Jpn. **37**, 912 (1974).
[38]G. van der Laan, C. Westra, C. Haas, and G. A. Sawatzky, Phys. Rev. B **23**, 4369 (1981).
[39]M. Taguchi, A. Chainani, N. Kamakura, K. Horiba, Y. Takata, M. Yabashi, K. Tamasaku, Y. Nishino, D. Miwa, T. Ishikawa, S. Shin, E. Ikenaga, T. Yokoya, K. Kobayashi, T. Mochiku, K. Hirata, and K. Motoya, Phys. Rev. B **71**, 155102 (2005).
[40]Frank de Groot and Akio Kotani, in *Advances in Condensed Matter Science*, edited by D. D. Sarma, G. Kotliar, and Y. Tokura (Taylor & Francis, New York, 2008), Vol. 6.
[41]T. Mizokawa, H. Namatame, A. Fujimori, K. Akeyama, H. Kondoh, H. Kuroda, and N. Kosugi, Phys. Rev. Lett. **67**, 1638 (1991).
[42]M. A. Korotin, V. I. Anisimov, D. I. Khomskii, and G. A. Sawatzky, Phys. Rev. Lett. **80**, 4305 (1998); D. Khomskii, Lithuanian Phys. J. **37**, 65 (1997).
[43]Katsuaki Sato, Yoshihisa Harada, Munetaka Taguchi, Shik Shin, and Atsushi Fujimori, Phys. Status Solidi A **206**, 1096 (2009).
[44]S. A. Carter, T. F. Rosenbaum, J. M. Honig, and J. Spalek, Phys. Rev. Lett. **67**, 3440 (1991).